

# ESI: Systematically investigating CO<sub>2</sub>:NH<sub>3</sub> ice mixtures using mid-IR and VUV spectroscopy - Part 1: thermal processing

Rachel L. James, Sergio Ioppolo, Søren V. Hoffmann, Nikola C. Jones, Nigel J. Mason and Anita Dawes

## S1 Experimental

### S1.1 The Open University Portable Astrochemistry Chamber set-up

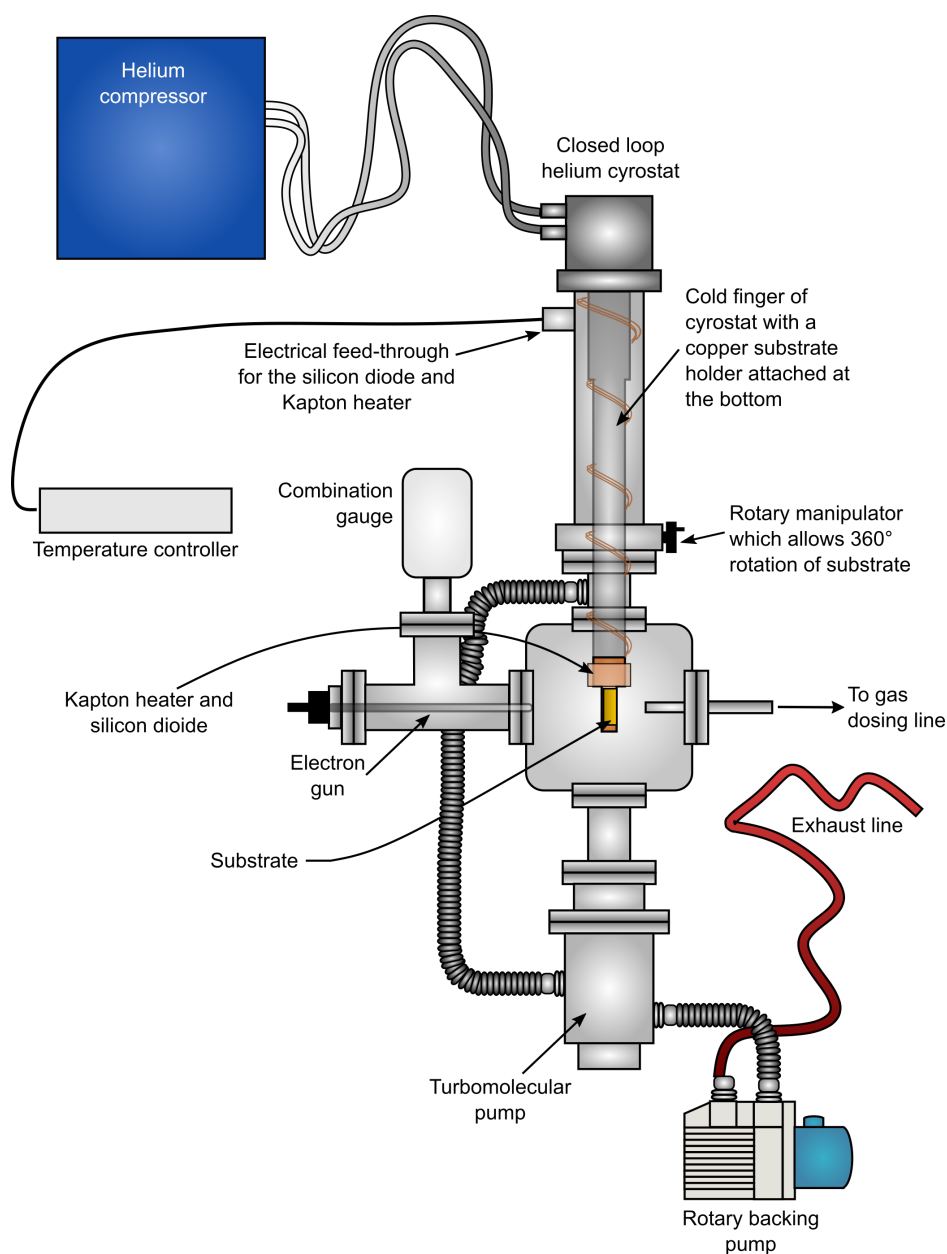
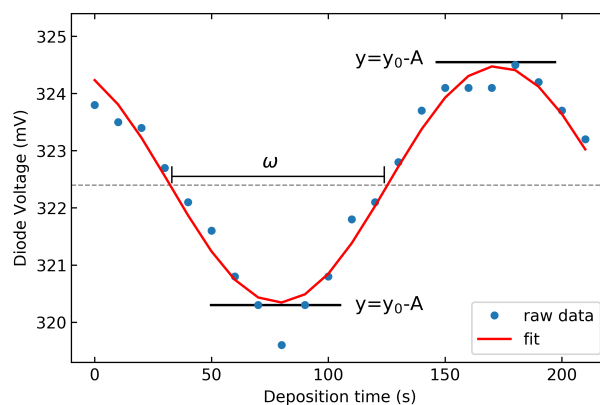


Figure S1 Schematic diagram of The Open University Portable Astrochemistry Chamber (PAC).

Fig. S1 shows a schematic diagram of the Portable Astrochemistry Chamber (PAC). The PAC is a spherical cube chamber (Kimball Physics MCF275-SC600-A) capable of achieving base pressures of low  $10^{-9}$  mbar via a turbomolecular pump (Leybold TURBOVAC TMP 151) backed by a two-stage oil rotary vane pump (Leybold TRIVAC D4B) when at a base temperature of 20 K. The pressure of the chamber was read from a combination gauge (Leybold Ionivac ITR 90) attached to a T-piece onto the chamber which also housed an electron gun which was not used in this study. A substrate holder (OFHC Cu, Goodfellow) attached to the cold head of a two-stage closed cycle helium cryostat (Sumitomo DE-202B) supplied by a helium compressor yielded a base temperature of 20 K. A silicon diode sensor (Lake Shore Cryosensors DT-670B-SD) positioned close to the substrate was used to read the temperature to within  $\pm 0.5$  K. Thermal processing was achieved via a Kapton flexible resistive heater (Omega) attached to the substrate holder and controlled using a temperature controller (Oxford Instruments Controller ITC 502). A differentially pumped rotary manipulator allowed the substrate holder to be rotated as required.

## S1.2 Film thickness

Prior to deposition the substrate was rotated so that it was at normal incidence to the gas inlet nozzle. During deposition the pressure in the PAC was regulated between  $1.0\text{--}1.2 \times 10^{-7}$  mbar via a high precision leak valve and *in situ* laser interferometry measurements were taken to estimate the ice thickness.



**Figure S2** *In situ* laser interferometry voltage measurements against deposition time. The raw data (blue circles) was fitted with Eq. 1 (red line). The  $y$ -offset ( $y_0$ ), phase shift ( $x_c$ ) half period ( $\omega$ ) and amplitude ( $A$ ) were obtained from the fit.

A HeNe laser beam ( $\lambda_0 = 632.8$  nm) was reflected off the surface of the ice sample at an incidence angle of  $20^\circ$  during film growth. Sinusoidal interference patterns due to reflection from the vacuum-ice surface and the ice film-substrate surface were measured with a photodiode and plotted as a function of voltage versus time. An example of this is shown in Fig. S2. The sinusoidal interference pattern was fitted using the following equation:

$$y = y_0 + A \sin\left(\pi \frac{x - x_c}{\omega}\right) \quad (1)$$

where  $y_0$  is the  $y$ -offset,  $x_c$  is the phase shift,  $A$  is the amplitude and  $\omega$  is the half period.

The refractive index of the ice film was estimated from the ratio of the minima to maxima of the fitted interference pattern<sup>1</sup>:

$$n_2 = \frac{y_0 + A}{y_0 - A} \quad (2)$$

The angle of the refracted beam was calculated using a rearranged form of Snell's Law:

$$\theta_2 = \sin^{-1}\left(\frac{n_1 \sin \theta_1}{n_2}\right) \quad (3)$$

where  $n_1$  is the refractive index of the vacuum ( $n_1 = 1$ ),  $\theta_1$  is the angle of incidence of the HeNe laser ( $\theta_1 = 20^\circ$ ) and  $n_2$  is the refractive index of the ice film estimated in Eq. 2.

The thickness of the ice per constructive interference fringe ( $d_f$ ) can then be calculated:

$$d_f = \frac{\lambda_0}{2n_2 \cos \theta_2} \quad (4)$$

**Table S1** Film thickness of samples used and normalisation factor applied. Mid-IR spectra were normalised to a thickness of 400 nm and VUV spectra were normalised to a thickness of 200 nm.

Spectroscopic study	Ratio	$d_s$ (nm)	Normalisation factor
Mid-IR	1:0	295	1.02
	3:1	380	0.79
	2:1	404	0.74
	1:1	400	0.75
	1:3	424	0.71
	1:10	403	0.74
	0:1	343	1.17
VUV	1:0	308	0.65
	4:1	284	0.70
	2:1	188	1.06
	1:3	140	1.43
	0:1	229	0.87

However, while all ice samples used in this work gave at least one complete interference fringe, as shown in Fig. S2, the sinusoidal interference pattern obtained for the ice sample thickness measurements were not necessarily comprised of an integer value of constructive fringes. Therefore, the deposition rate ( $r$ ) was calculated using the period ( $2\omega$ ):

$$r = \frac{d_f}{2\omega} \quad (5)$$

Using the deposition time ( $t$ ), the thickness of the ice sample ( $d_s$ ) is given as:

$$d_i = \frac{rt}{\sin(45)} \quad (6)$$

where  $\sin(45)$  is the thickness correction due to the substrate being held at a 45° to the IR beam for all mid-IR spectra acquisition.

Table S1 gives the film thickness for pure CO<sub>2</sub>, pure NH<sub>3</sub> and CO<sub>2</sub>:NH<sub>3</sub> mixtures after deposition at 20 K. A thickness normalisation factor was applied when different ratios were compared.

### S1.3 Determining the mid-IR CO<sub>2</sub>:NH<sub>3</sub> ratios

The ratios of the CO<sub>2</sub>:NH<sub>3</sub> mixtures were determined from the column densities of CO<sub>2</sub> and NH<sub>3</sub> which were calculated from the mid-IR absorption spectra. The column density of molecular species  $i$  ( $N_i$ ) is calculated via the following equation:

$$\tau = \ln \left( \frac{I_0(\tilde{\nu})}{I_t(\tilde{\nu})} \right) = \sigma(\tilde{\nu})N_i \quad (7)$$

where  $\tau(\tilde{\nu})$  is the optical depth at a given wavenumber  $\tilde{\nu}$  which is calculated from the incident ( $I_0(\tilde{\nu})$ ) and transmitted ( $I_t(\tilde{\nu})$ ) intensities and  $\sigma(\tilde{\nu})$  is the cross section at a given wavenumber  $\tilde{\nu}$  (cm<sup>2</sup>).

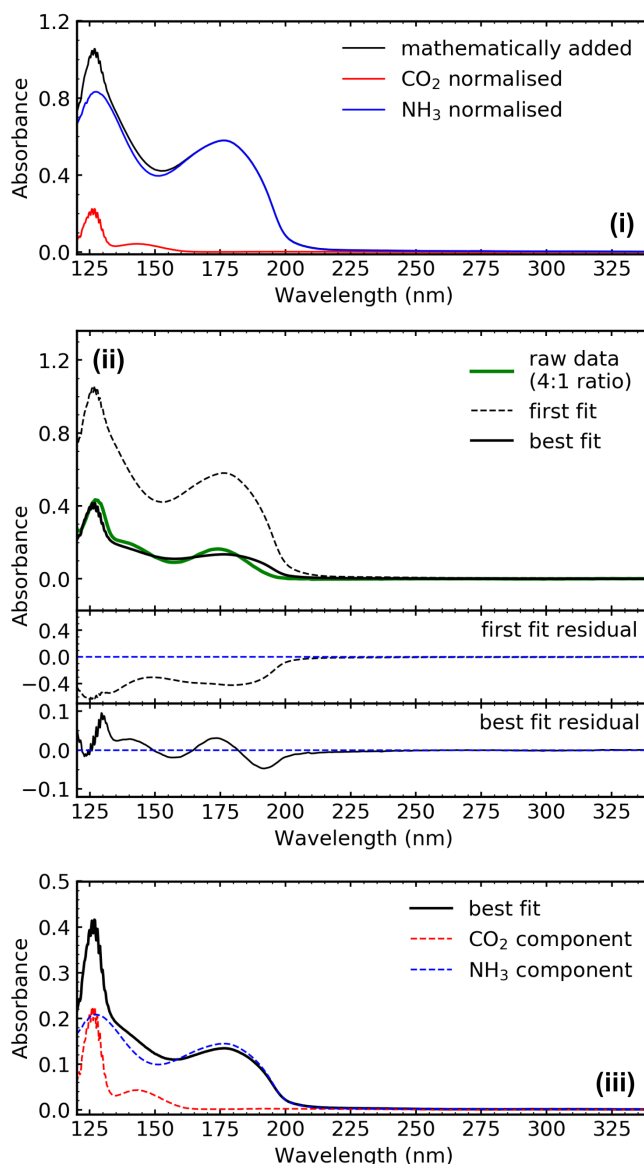
Mid-IR spectra were obtained in absorbance (log scale) and converted to optical depth (ln scale) by multiplication of  $\ln(10)$ . The column density of a specific vibrational mode of molecular species  $i$  was then obtained by integrating Eq. 7:

$$N_i = \frac{1}{A'_i} \int \tau(\tilde{\nu}) d\tilde{\nu} \quad (8)$$

where  $A'_i = \int \sigma(\tilde{\nu}) d\tilde{\nu}$  (cm molecule<sup>-1</sup>) is the infrared apparent band strength of a specific vibrational mode which is constant and obtained from the literature and  $\int \tau(\tilde{\nu}) d\tilde{\nu}$  is the area of the specific vibrational absorption band.

The CO<sub>2</sub> column density was determined from the  $\nu_3$  absorption band near 2340 cm<sup>-1</sup> using an  $A'_i$  of  $7.6 \times 10^{-17}$  cm molecule<sup>-12</sup> and an integration range between 2400–2300 cm<sup>-1</sup>. The NH<sub>3</sub> column density was determined from the  $\nu_2$  absorption band near 1070 cm<sup>-1</sup> using an  $A'_i$  of  $1.63 \times 10^{-17}$  cm molecule<sup>-12</sup> and an integration range between 1250–950 cm<sup>-1</sup>.

We note that the band strength of molecules can be influenced by the matrix in which they reside such that the CO<sub>2</sub> band strength in a 4:1 ratio may be different to the 1:10 ratio. Therefore the  $A'_i$  which was obtained from the literature for the pure ices, can introduce errors of up to  $\pm 40\%$  uncertainty into the ratio calculation.<sup>3</sup>

S1.4 Determining the VUV  $\text{CO}_2:\text{NH}_3$  ratios

**Figure S3** Method for determining the ratio of a  $\text{CO}_2:\text{NH}_3$  mixture from a VUV spectrum. **(i)** VUV spectra of  $\text{CO}_2$  and  $\text{NH}_3$  were normalised to the same thickness of 200 nm (red =  $\text{CO}_2$ , blue =  $\text{NH}_3$ ) and then mathematically added together (black). **(ii)** The first fit (black dashed) was the mathematical spectrum from (i) which was fitted to the raw data (green) and the first fit residual was analysed. The best fit (black solid) was obtained through a manual iterative process which brought the positive and negative components of the residual closest to zero and is shown in the best fit residual. **(iii)** The  $\text{CO}_2$  and  $\text{NH}_3$  components which make up the best fit can be extracted. In this case the  $\text{CO}_2$  component (red dashed) was  $\times 1.00$  that of the normalised  $\text{CO}_2$  spectrum and the  $\text{NH}_3$  component (blue dashed) was  $\times 0.23$  that of the normalised  $\text{NH}_3$  spectrum so an approximate  $\text{CO}_2:\text{NH}_3$  ratio of 4:1 was obtained.

To determine the  $\text{CO}_2$  ratios directly from VUV spectra, the ratios of the  $\text{CO}_2$  and  $\text{NH}_3$  mixtures were approximated by mathematically adding the VUV spectrum of a pure  $\text{NH}_3$  ice and a pure  $\text{CO}_2$  ice, analysing the residual and iterating until a best fit was found. A detailed explanation on how the ratios of the VUV spectra were calculated using this approximation is given below:

1. A VUV spectrum of pure  $\text{CO}_2$  ice and a VUV spectrum of pure  $\text{NH}_3$  ice were normalised to the same thickness, in this case the arbitrary thickness of 200 nm was chosen.
2. The pure spectrum of  $\text{CO}_2$  ice and the pure spectrum of  $\text{NH}_3$  ice were mathematically added together.

3. The mathematical spectrum was then fitted to a spectrum of a CO<sub>2</sub>:NH<sub>3</sub> mixture and the residual was analysed.
4. The best fit was obtained through an iterative process which brought the sum of the positive and negative components of the residual closest to zero. The best fit residual contained both positive and negative components due to shifts in the positions of electronic transition bands and changes in the widths of the electronic transitions bands.
5. From the best fit the CO<sub>2</sub> and NH<sub>3</sub> components were extracted which were given as fractional values of the normalised CO<sub>2</sub> and NH<sub>3</sub> from step 1. The ratio of the CO<sub>2</sub>:NH<sub>3</sub> mixture was determined from these fractions.

An example of this method is shown in Fig. S3 for the 4:1 ratio. A ratio of approximately 3:1 was expected for this mixture as during mixing the ratio of the partial pressures of CO<sub>2</sub> and NH<sub>3</sub> mixed in the gas line were the same as the ratio of the partial pressures which were used in the mid-IR study. The other ratios obtained for the VUV spectroscopic study were 2:1 and 1:3.

## S2 Additional mid-IR results

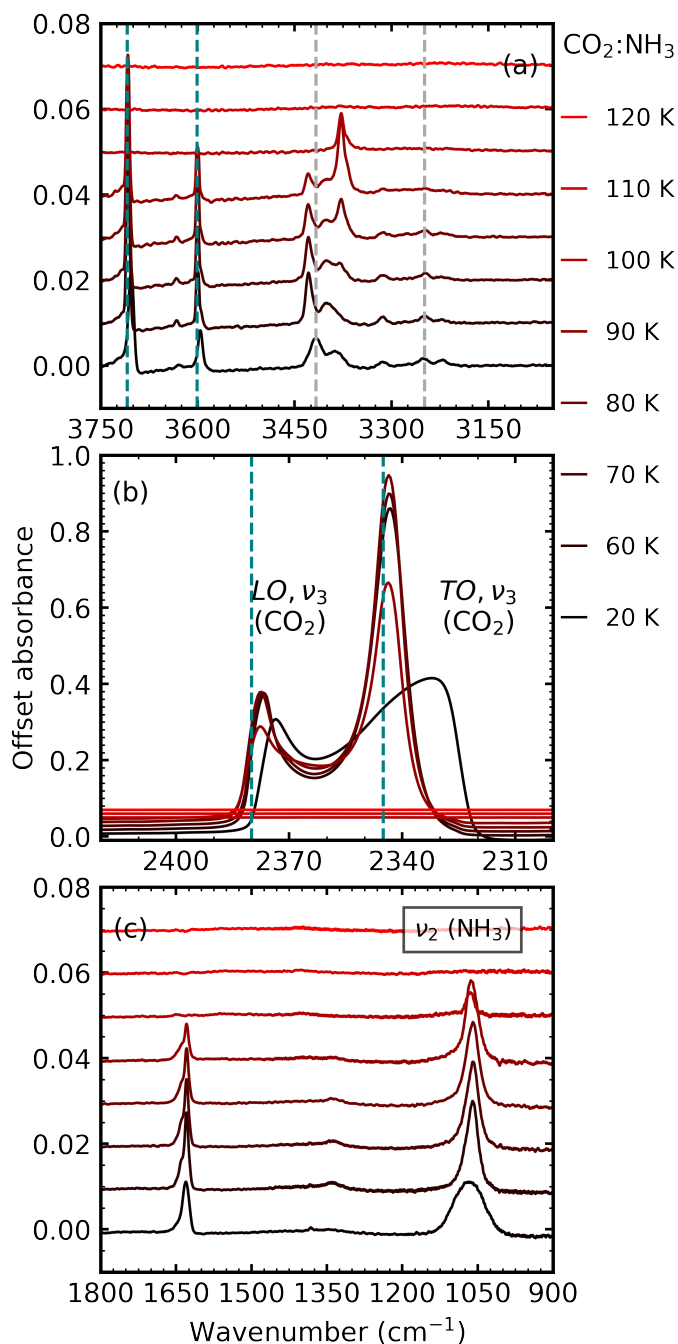


**Figure S4** Mid-IR spectra of the thermal processing results of a CO<sub>2</sub>:NH<sub>3</sub> mixture in a 3:1 ratio from 20 to 250 K. Spectra are offset on the y-axis for clarity. **(a)** Segregation of the mixture was observed through the shift in the position of the CO<sub>2</sub> absorption bands towards the position of pure CO<sub>2</sub> absorption bands when deposited at 20 K which are indicated by blue dashed lines. Grey dashed lines indicate the CO<sub>2</sub>:NH<sub>3</sub> molecular complex absorption bands which disappeared between 70–80 K. **(b)** LO-TO splitting of the ν<sub>3</sub> absorption band of CO<sub>2</sub>. Segregation of the mixture was observed through the shift in the position of the LO and TO modes towards pure CO<sub>2</sub> positions which are indicated by blue dashed lines. **(c)** A phase change was observed for NH<sub>3</sub> through the splitting of the ν<sub>2</sub> absorption band between 70–80 K. No new bands observed between 1800–1200 cm<sup>-1</sup> at 80 K.

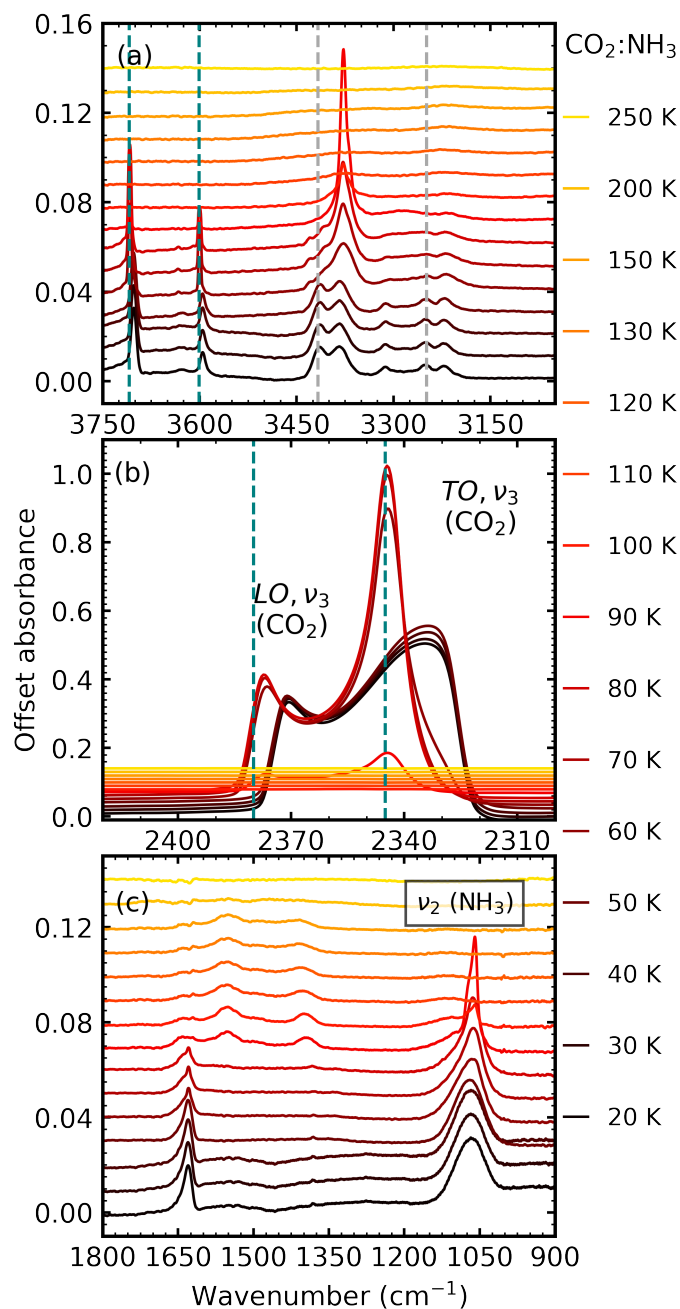


**Figure S5** Mid-IR spectra of the thermal processing results of a CO<sub>2</sub>:NH<sub>3</sub> mixture in a 2:1 ratio from 20 to 250 K. Spectra are offset on the y-axis for clarity. **(a)** Segregation of the mixture was observed through the shift in the position of the CO<sub>2</sub> absorption bands towards the position of pure CO<sub>2</sub> absorption bands when deposited at 20 K which are indicated by blue dashed lines. Grey dashed lines indicate the CO<sub>2</sub>:NH<sub>3</sub> molecular complex absorption bands which disappeared between 70–80 K. **(b)** LO-TO splitting of the ν<sub>3</sub> absorption band of CO<sub>2</sub>. Segregation of the mixture was observed through the shift in the position of the LO and TO modes towards pure CO<sub>2</sub> positions which are indicated by blue dashed lines. **(c)** A phase change was observed for NH<sub>3</sub> through the splitting of the ν<sub>2</sub> absorption band between 70–80 K. New bands between 1800–1200 cm<sup>-1</sup> at 80 K indicated thermal reaction.

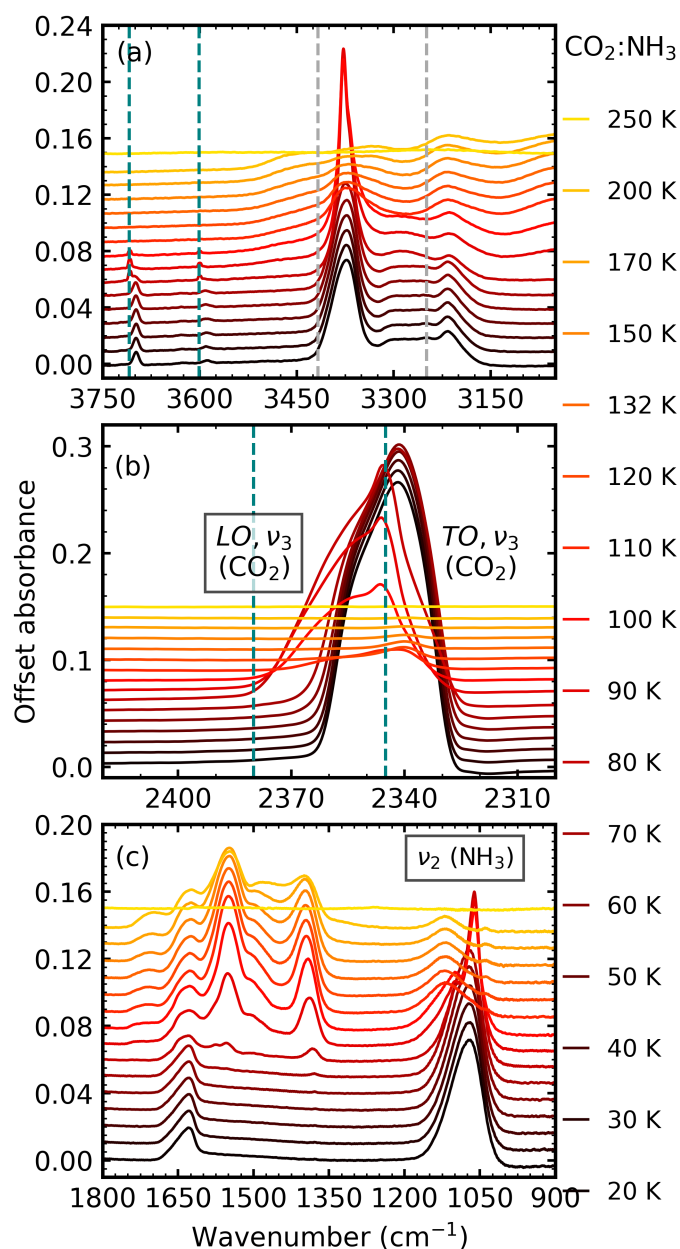


**Figure S6** Mid-IR spectra of the thermal processing results of a  $\text{CO}_2:\text{NH}_3$  mixture in a 1:3 ratio from 20 to 250 K. Spectra are offset on the y-axis for clarity. **(a)** Segregation of the mixture was observed through the shift in the position of the  $\text{CO}_2$  absorption bands towards the position of pure  $\text{CO}_2$  absorption bands when deposited at 20 K which are indicated by blue dashed lines. Grey dashed lines indicate the  $\text{CO}_2:\text{NH}_3$  molecular complex absorption bands which disappeared between 70–80 K. **(b)** LO-TO splitting of the  $\nu_3$  absorption band of  $\text{CO}_2$ . Segregation of the mixture was observed through the shift in the position of the LO and TO modes towards pure  $\text{CO}_2$  positions which are indicated by blue dashed lines. **(c)** A phase change was observed for  $\text{NH}_3$  through the splitting of the  $\nu_2$  absorption band between 70–80 K. New bands between 1800–1200  $\text{cm}^{-1}$  at 80 K indicated thermal reaction.

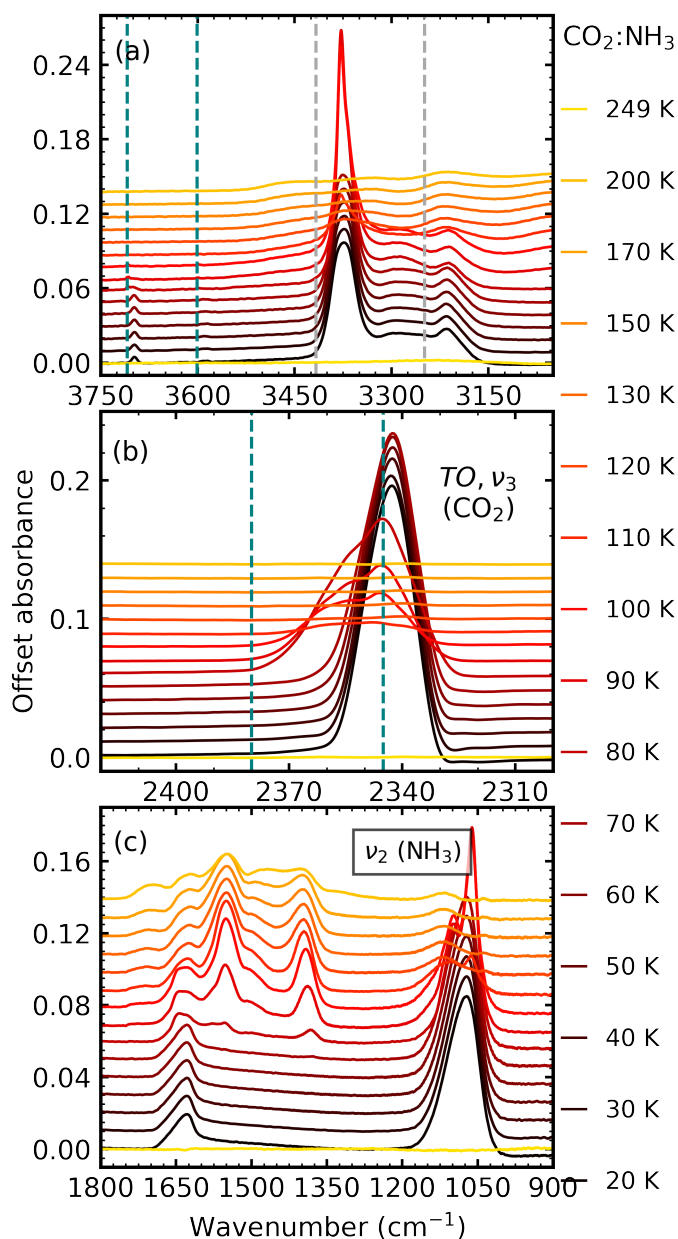


**Figure S7** Mid-IR spectra of the thermal processing results of a CO<sub>2</sub>:NH<sub>3</sub> mixture in a 1:10 ratio from 20 to 250 K. Spectra are offset on the y-axis for clarity. **(a)** Segregation of the mixture was observed through the shift in the position of the CO<sub>2</sub> absorption bands towards the position of pure CO<sub>2</sub> absorption bands when deposited at 20 K which are indicated by blue dashed lines. Grey dashed lines indicate the CO<sub>2</sub>:NH<sub>3</sub> molecular complex absorption bands which disappeared between 70–80 K. **(b)** LO-TO splitting of the ν<sub>3</sub> absorption band of CO<sub>2</sub>. Segregation of the mixture was observed through the shift in the position of the LO and TO modes towards pure CO<sub>2</sub> positions which are indicated by blue dashed lines. **(c)** A phase change was observed for NH<sub>3</sub> through the splitting of the ν<sub>2</sub> absorption band between 70–80 K. New bands between 1800–1200 cm<sup>-1</sup> at 80 K indicated thermal reaction.

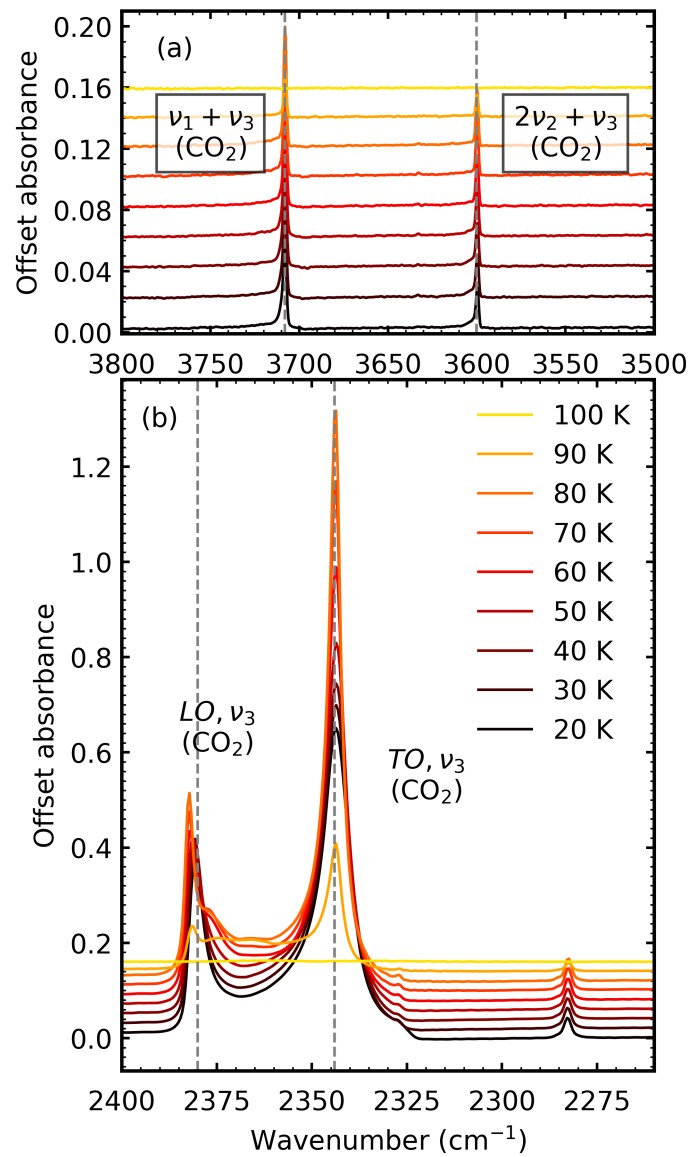


**Figure S8** Mid-IR spectra of the thermal processing results of a pure CO<sub>2</sub> ice from 20 to 100 K for (a) combination modes and (b) LO-TO splitting of the  $\nu_3$  absorption band. Dashed lines indicate the position of the CO<sub>2</sub> absorption bands at 20 K. Spectra are offset on the y-axis for clarity.

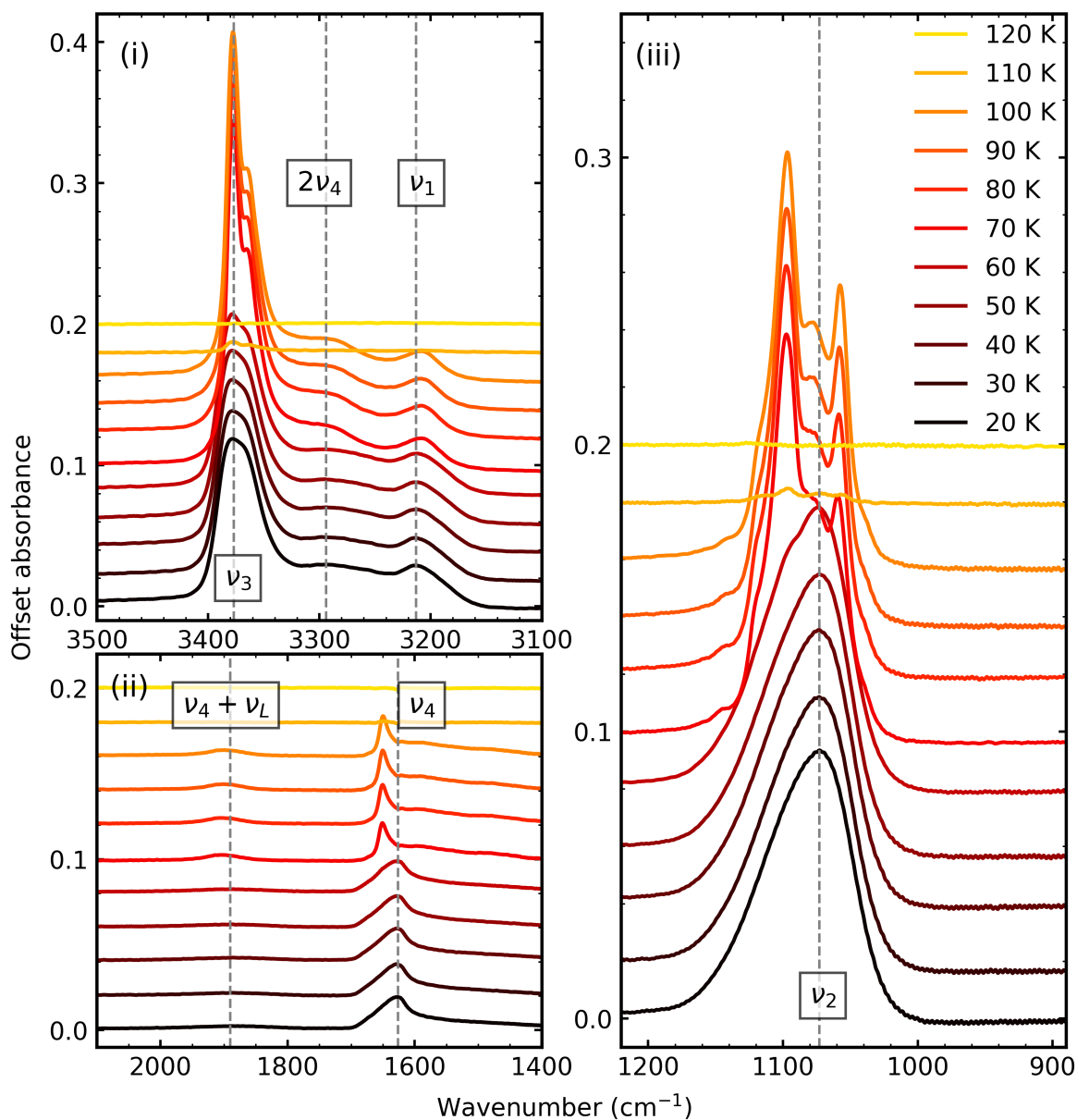


**Figure S9** Mid-IR spectra of the thermal processing results of a pure NH<sub>3</sub> ice from 20 to 120 K for (a)  $\nu_3$ ,  $2\nu_4$  &  $\nu_1$  vibrational modes; (b)  $\nu_4 + \nu_L$  &  $\nu_4$  absorption bands and (c)  $\nu_2$  absorption band. Dashed lines indicate the position of the NH<sub>3</sub> absorption bands at 20 K. Spectra are offset on the y-axis for clarity.

**Table S2** Summary of the multiple IR assignments of the same vibrational modes throughout the literature of the thermal processing of CO<sub>2</sub>:NH<sub>3</sub> mixtures. \* No vibrational mode assigned, asym = asymmetric, sym. = symmetric, oop = out of plane, AC = ammonium carbamate, CA = carbamic acid.

Range (cm <sup>-1</sup> )	Frasco <sup>4</sup>	Hitsatsune <sup>5</sup>	Bossa <i>et al.</i> <sup>6</sup>	Rodríguez-Lazcano <i>et al.</i> <sup>7</sup>
829–833	NCO <sub>2</sub> oop bend	CO <sub>2</sub> wag	OCN oop bend (AC)	NH <sub>2</sub> twist (CA)
1035–1040	NH <sub>2</sub> wag	NH <sub>2</sub> rock	NH <sub>2</sub> wag (AC)	C–N stretch (AC and CA)
1114–1122	CO <sub>2</sub> sym. str.	C–N stretch	C–N stretch (AC)	NH <sub>2</sub> rock (AC)
1261–1265	NH <sub>2</sub> wag	NH <sub>2</sub> rock		
1397–1404	C–N stretch	COO <sup>-</sup> sym. Stretch	COO <sup>-</sup> sym stretch (AC)	COO <sup>-</sup> sym. Stretch (AC)
1445–1451	C–N stretch	NH <sub>4</sub> <sup>+</sup> bend	CA dimer	
1460–1500	NH <sub>4</sub> <sup>++*</sup>	NH <sub>4</sub> <sup>+</sup> bend	NH <sub>4</sub> <sup>+</sup> bend (AC)	C–O stretch (CA)
1543–1553	COO <sup>-</sup> asym stretch	COO <sup>-</sup> asym stretch	COO <sup>-</sup> asym stretch (AC)	COO <sup>-</sup> asym stretch (AC)
1623–1628	N–H bend	N–H bend	N–H bend (AC)	NH <sub>4</sub> <sup>+</sup> bend (AC)
1691–1705			C=O stretch (CA)	C=O stretch (AC)
1940–1983	NH <sub>4</sub> <sup>+</sup> combination	NH <sub>4</sub> <sup>+</sup> stretch		combination (AC)
2172–2236	COO <sup>-</sup> sym stretch overtone	NH <sub>4</sub> <sup>+</sup> stretch (× 2)		combination (AC)
2747–3089	NH <sub>4</sub> <sup>++*</sup>	NH <sub>4</sub> <sup>+</sup> stretch (× 3)		NH <sub>4</sub> <sup>+</sup> stretch (× 2) (AC)
3140 (broad)			O–H stretch (CA)	
3120–3365	N–H sym stretch (× 2)	N–H sym stretch (× 3)	aceNH <sub>2</sub> stretch (AC)	2 assignments, NH <sub>2</sub> asym stretch and NH <sub>2</sub> sym stretch (AC)
3415–3475	N–H asym stretch	N–H asym stretch	NH <sub>2</sub> stretch (AC and CA)	NH <sub>2</sub> asym stretch or O–H stretch (AC or CA)

## S3 Additional thermal processing VUV spectra

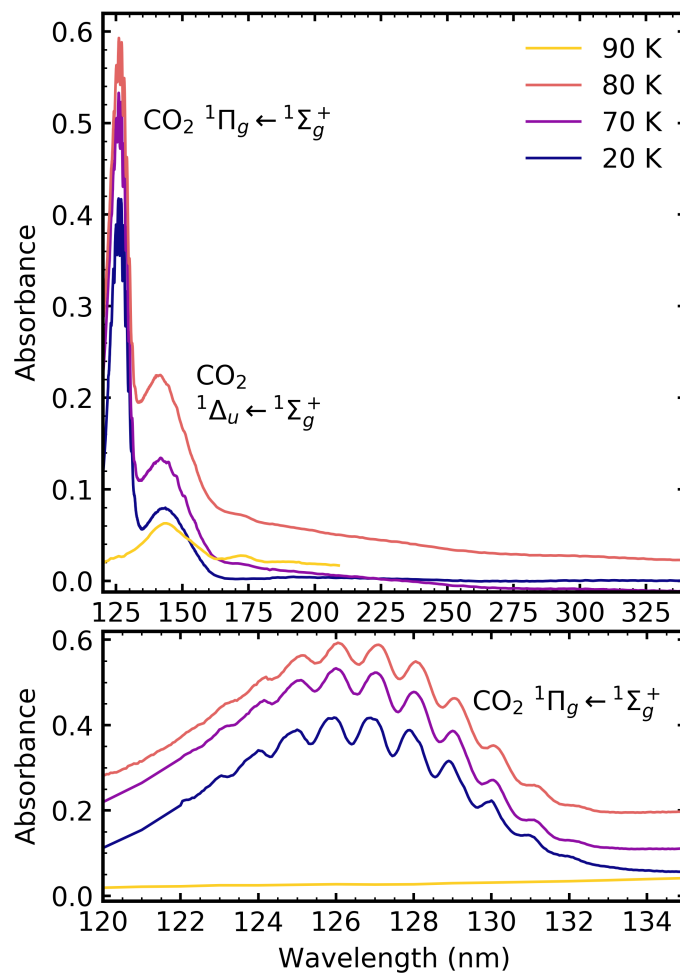


**Figure S10** VUV spectra of the thermal processing of a pure CO<sub>2</sub> mixture from 20–90 K between 120–340 nm (top plot). Bottom plot shows the vibrational structure of the CO<sub>2</sub>  $^1\Pi_g \leftarrow \ ^1\Sigma_g^+$  transition between 120–135 nm. Note, at 90 K CO<sub>2</sub> was desorbing and absorption spectra was only obtained between 120–220 nm.

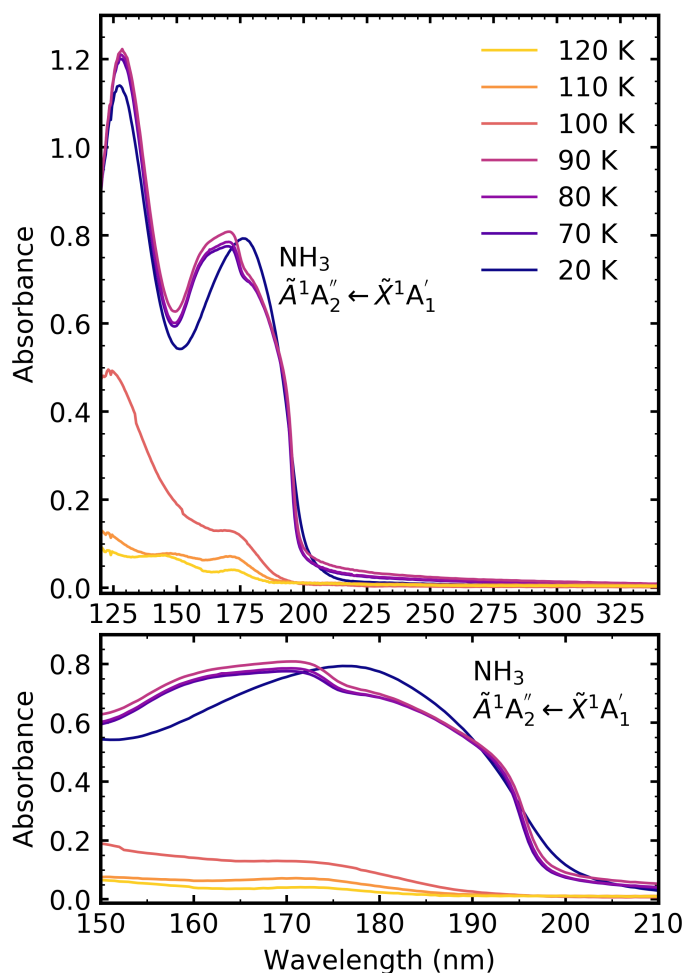


**Figure S11** VUV spectra of the thermal processing of a pure NH<sub>3</sub> mixture from 20–120 K between 120–340 nm (top plot). Bottom plot NH<sub>3</sub>  $\tilde{A}^1A_2'' \leftarrow \tilde{X}^1A_1'$  transition between 150–210 nm.

## Notes and references

- [1] M. S. Westley, G. A. Baratta and R. A. Baragiola, *J. Chem. Phys.*, 1998, **108**, 3321–3326.
- [2] M. Bouilloud, N. Fray, Y. Bénilan, H. Cottin, M.-C. Gazeau and A. Jolly, *Mon. Not. R. Astron. Soc.*, 2015, **451**, 2145–2160.
- [3] J. Terwisscha van Scheltinga, N. F. W. Ligterink, A. Boogert, E. van Dishoeck and H. Linnartz, *Astron. Astrophys.*, 2018, **611**, A35.
- [4] D. Frasco, *J. Chem. Phys.*, 1964, **41**, 2134–2140.
- [5] I. C. Hisatsune, *Can. J. Chem.*, 1983, **62**, 945–948.
- [6] J. B. Bossa, F. Duvernay, P. Theulé, F. Borget and T. Chiavassa, *Chem. Phys.*, 2008, **354**, 211–217.
- [7] Y. Rodríguez-Lazcano, B. Maté, V. J. Herrero, R. Escribano and Ó. Gálvez, *Phys. Chem. Chem. Phys.*, 2014, **16**, 3371–3380.